

**Keywords:** alkaline phosphatase; trace metal binding; chelating drug compounds; Langmuir–Blodgett monolayer; X-ray fluorescence; X-ray total external reflection.

# Distinct effect of xenobiotics on the metal-binding properties of protein molecules

Natalia Novikova,<sup>a,\*</sup> Mikhail Kovalchuk,<sup>a</sup> Nina Stepina,<sup>b</sup> Radmir Gaynutdinov,<sup>b</sup> Elena Chukhrai<sup>c</sup> and Eleonora Yurieva<sup>d</sup>

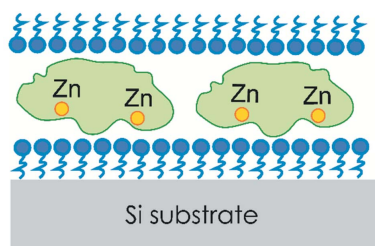
<sup>a</sup>National Research Centre 'Kurchatov Institute', Akademika Kurchatova pl. 1, Moscow 123182, Russia, <sup>b</sup>Shubnikov Institute of Crystallography, Russian Academy of Sciences, Leninskii pr. 59, Moscow 119333, Russia, <sup>c</sup>Department of Chemistry, Lomonosov Moscow State University, GSP-1, Leninskie Gory, Moscow 119991, Russia, and <sup>d</sup>Institute of Pediatrics and Pediatric Surgery, Russian Academy of Medical Sciences, Taldomskaya str. 2, Moscow 125412, Russia. \*Correspondence e-mail: nn-novikova07@yandex.ru

The X-ray standing-wave method was applied to study the elemental composition and molecular organization of ordered protein films of alkaline phosphatase exposed to different xenobiotics (drug compounds, lead). Binding of metal ions from triply distilled water to protein molecules has been experimentally observed. Definite differences in the arrangement of impurity metal ions in the films have been established. The considerable enhancement of protein–metal interactions is attributed to partial rearrangement of the protein native structure, induced by xenobiotics.

## 1. Introduction

Metals perform exceptionally important biochemical functions in living organisms; primarily these are the stabilization of folded proteins and the regulation of catalytic properties of enzymes. While an impressive array of modern physico-chemical methods has been applied to elucidate the role of metals in biological systems, many mechanisms that govern protein–metal interactions remain unknown. It is evident that the efficiency of research in this area depends, to a large extent, on new physical methods that would enable an understanding of the interaction mechanisms at the molecular level.

Modern high-resolution X-ray methods are especially advantageous for characterization of bioorganic nanosystems. The rapid progress of high intensive X-ray sources, such as synchrotrons, brought these studies to a fundamentally new level; many X-ray methods traditionally used for structural diagnostics of bulk solid samples have been extended for investigations of weakly scattering bioorganic molecules. The X-ray standing-wave (XSW) method is well known as a very precise technique that allows low signal to be separated from a small number of atoms due to the spectral selectivity of fluorescence measurements (Batterman, 1964; Kovalchuk & Kohn, 1986; Vartanyants & Kovalchuk, 2001). XSW studies are based on simultaneous measurements of the angular dependence of the X-ray reflectivity and the intensity of the fluorescence yield emitted from the sample under Bragg diffraction or total external reflection when a high intensive reflected wave is generated in the sample. The key idea of the XSW method is that the shape of the angular dependence of the fluorescence yield is very sensitive to the position of the atoms emitting the fluorescence radiation. This offers the opportunity to locate the atoms along the normal of the



sample surface from analysis of the corresponding fluorescence curve. In addition, due to the element sensitivity of fluorescence measurements, the position of several types of atoms inside the film can be studied individually.

The great potential of the XSW technique for determining the position of metal atoms inside the ordered organic films has been demonstrated elsewhere (see, for example, Iida *et al.*, 1985; Bedzyk *et al.*, 1988; Zheludeva *et al.*, 2001; Libera *et al.*, 2005). XSW measurements under total external reflection (TER) have been used by Templeton *et al.* (2001) to investigate trace metal sorption in biofilms of chemoorganotrophic bacterium deposited on single-crystal substrates ( $\text{Al}_2\text{O}_3$  and  $\text{Fe}_2\text{O}_3$ ). The data obtained in this experiment provide detailed information on the partitioning of lead at the biofilm/metal oxide interfaces.

The long-period standing wave generated under TER conditions is an ideal 'scale ruler' for studying large protein molecules. By changing the incident angle, one can literally scan protein molecules deposited on the surface of an X-ray mirror by the wavefield to directly locate the binding site of atoms of a specific kind. One of the first measurements of this kind was reported by Wang *et al.* (1994) where XSW measurements were carried out to investigate the protein cytochrome c immobilized on silver mirrors.

In our recent experiments the XSW method has been applied to elucidate the effect of different toxic reagents (urea and heavy metals) on the protein–lipid interaction (Novikova *et al.*, 2011). Protein films of glucose oxidase formed on the liquid surface have been studied. These measurements revealed a noticeable increase in the ability of glucose oxidase molecules to bind metals after incubation in 0.09 M urea solution. A similar phenomenon has been observed in our measurements of protein specimens extracted from the urine of children with different metabolic diseases (Novikova *et al.*, 2012). Element composition of protein specimens was determined by total reflection X-ray fluorescence analysis (TXRF). We examined 340 patients with various metabolic disorders. The presence of metal ions (Fe, Zn, Cu, Ni) was clearly detected in the majority of cases. It was supposed that pathological products of metabolism (homocysteine and intermediate molecules) and physiological products of metabolism in high doses (urea, uric acid, hormones, neuro-mediators and peroxidation products), as well as various xenobiotics (including drugs), act as toxic agents resulting in the enhancement of the metal-binding properties of protein molecules analogous to that observed in the model experiments on glucose oxidase.

These results have initiated our further studies, and in the experiments reported here we investigated the effect of different xenobiotics on the metal-binding properties of the protein alkaline phosphatase. The XSW method has been used for determining the element composition and molecular organization of the ordered films of alkaline phosphatase exposed to solutions of three chelating drug compounds at high (compared with therapeutic doses) concentrations. For comparison, the action of a toxic reagent (lead) has been also examined.

## 2. Materials and methods

### 2.1. Deposition of protein films on solid substrates

The immobilization of alkaline phosphatase (AP) on solid substrates was carried out by the method of protein adsorption on a surfactant monolayer preliminary deposited onto a solid substrate. Two different surfactants have been used: a natural polymer cellulose acetopivalinate (CAP) and a lipid (L) mixture phosphatidylcholine/cholesterol (in a molar ratio of 7:3).

We used the following reagents: alkaline phosphatase from porcine kidney lyophilized powder containing approximately 90% of protein (100–300 DEA units per mg protein); 1,2-dipalmitoyl-*sn*-glycero-3-phosphatidylcholine (DPPC), cholesterol, three chelating compounds [ethylenediamine-tetraacetic acid (EDTA), succimer, xydiphone] and the polymer cellulose acetopivalinate. Alkaline phosphatase, DPPC, cholesterol, EDTA and succimer were purchased from Sigma, USA. The drug compound xydiphone (a bisphosphonate chelating agent) was a product of Moskhimpreparat Ltd, Russia. Cellulose acetopivalinate was synthesized at the Institute of macromolecular compounds (St Petersburg, Russia).

The general scheme of protein deposition was as follows: a polymer or lipid monolayer was transferred onto hydrophobic substrates by the vertical lifting (Langmuir–Blodgett) method. As substrates we used standard commercial silicon wafers (SI) treated by dimethyldichlorosilane solution. A lyophilized powder of protein was dissolved in a Tris HCl buffer solution (pH 8.3). The silicon substrate with Langmuir–Blodgett monolayer was placed into a vessel filled with the protein solution. The immobilization of AP was performed from the working protein solution with a protein concentration of  $0.250 \text{ mg l}^{-1}$  at room temperature for 15 h. Then the vessel was placed on the bottom of a Langmuir trough filled with triply distilled water. A lipid or polymer monolayer was formed on the surface of a water subphase, and the substrate with the immobilized protein layer was withdrawn through the monolayer. The final film was composed of three layers: the surfactant monolayer as bottom and top layers, and the protein monolayer in the middle of the film. The side view of the protein film is presented in Fig. 1(a). The overall structure of alkaline phosphatase is shown in Fig. 1(b). Three series of samples have been deposited.

**2.1.1. Series I: control samples.** *Sample N1.* (SI-L)+AP. Alkaline phosphatase was immobilized onto a lipid monolayer.

*Sample N2.* (SI-CAP)+AP. Alkaline phosphatase was immobilized onto a polymer monolayer.

**2.1.2. Series II.** Series II was devoted to the studies of the action of chelating drug compounds at high concentrations which are toxic compared with therapeutic doses. In this case chelating agents (EDTA, succimer or xydiphone) were added to the solution of AP. The mixture was incubated for 2 h. The immobilization of the protein onto a phosphatidylcholine/cholesterol monolayer was carried out according to the general scheme.

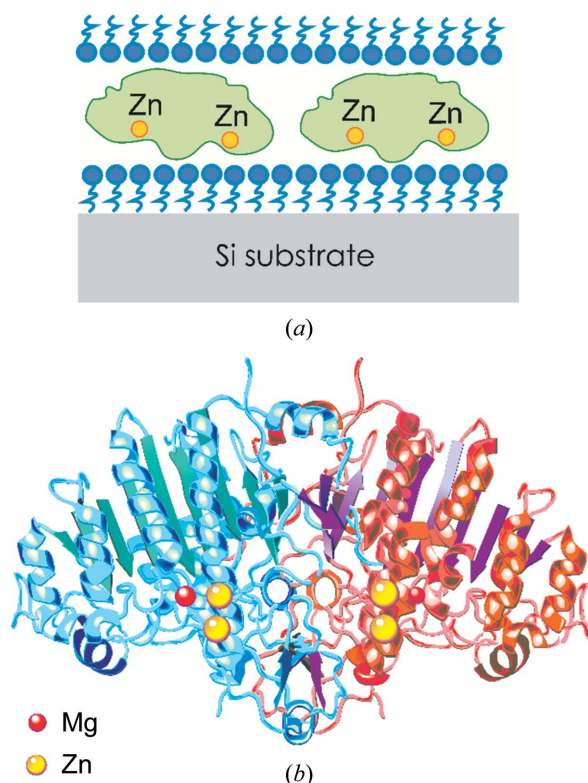


**Figure 1**  
Schematic view of the deposited protein film (a). The overall structure of alkaline phosphatase; the Zn ions bound in the active site are indicated by yellow balls (b).

*Sample N3.* (SI-L)+AP[EDTA]. The concentration of EDTA in the solution was 0.04%.

*Sample N4.* (SI-L)+AP[succimer]. The concentration of succimer in the solution was 0.02%.

*Sample N5.* (SI-L)+AP[xydiphone]. The concentration of xydiphone in the solution was 2%.

**2.1.3. Series III.** For comparison, the effect of lead solution on the AP molecules has been also examined.

*Sample N6.* {(SI-CAP)+AP}[Pb]. The immobilization of the protein onto a monolayer of cellulose acetopivalinate was carried out according to the general scheme, but, after the formation of the protein layer, the sample was incubated for 3 h in a lead acetate solution at a concentration of  $3 \times 10^{-4}$  M. Then the substrate containing the immobilized protein layer was withdrawn through the cellulose acetopivalinate monolayer.

*Sample N7.* {(SI-L)+AP}[Pb]. Sample N7 was prepared by analogy with sample N6 but this time phosphatidylcholine/cholesterol monolayer was used as the immobilizing layer; besides, the concentration of lead acetate was substantially lower ( $3 \times 10^{-6}$  M).

All protein films under investigation are listed in Table 1.

## 2.2. X-ray fluorescence measurements

Experimental measurements were performed at the KMC-2 beamline at the BESSY synchrotron radiation facility (Germany). The energy of the incident beam was 13.5 keV.

**Table 1**  
Protein films investigated.

N	Description of sample	Abbreviation	Serial number of experiments
1	AP adsorbed on a lipid monolayer (SI-L)	(SI-L)+AP	Series I
2	AP adsorbed on cellulose acetopivalinate monolayer (SI-CAP)	(SI-CAP)+AP	
3	Complex of AP with the chelating agent EDTA adsorbed on a lipid monolayer (SI-L)	(SI-L)+AP[EDTA]	Series II
4	Complex of AP with the chelating agent succimer adsorbed on a lipid monolayer (SI-L).	(SI-L)+AP[succimer]	
5	Complex of AP with the chelating agent xydiphone adsorbed on a lipid monolayer (SI-L).	(SI-L)+AP[xydiphone]	
6	AP was adsorbed on cellulose acetopivalinate monolayer (SI-CAP) and exposed to a lead acetate solution at a concentration of $3 \times 10^{-4}$ M	{(SI-CAP)+AP}[Pb]x	Series III
7	AP was adsorbed on a lipid monolayer (SI-L) and exposed to a lead acetate solution at a concentration of $3 \times 10^{-6}$ M	{(SI-L)+AP}[Pb]x	

The characteristic fluorescence spectra were recorded for each angle of incidence in the angle range corresponding to the TER region of silicon.

## 2.3. Atomic force microscopy measurements

In order to examine the surface morphology of the deposited protein films, additional atomic force microscopy (AFM) studies have been performed. The measurements were carried out at the atomic force microscope P47-SPM-MDT (Russia, NT-MDT) in the tapping mode. NSC11 silicon cantilevers (Mikromasch, Estonia) with a point radius  $R < 10$  nm were used.

## 3. Results and discussion

### 3.1. Studies of element composition

Fig. 2 shows typical characteristic fluorescence spectra from control protein films of AP recorded at angles smaller than the critical angle of total external reflection for silicon substrate  $\theta_C = 2.34$  mrad. Although the most intense peaks on these spectra are Ar  $K_\alpha$  and Si  $K_\alpha$  from argon of the surrounding atmosphere and silicon from the substrate, a distinct Zn  $K_\alpha$  peak from zinc ions bound in the active site of the AP molecule is clearly visible. The intensity of the Zn  $K_\alpha$  peak on the spectrum from sample N2 (SI-CAP)+AP (the protein molecules are immobilized onto the monolayer of cellulose acetopivalinate) is much higher than that on the spectrum from sample N1 (SI-L)+AP (the protein molecules are immobilized onto a lipid monolayer). This can be explained by the stronger

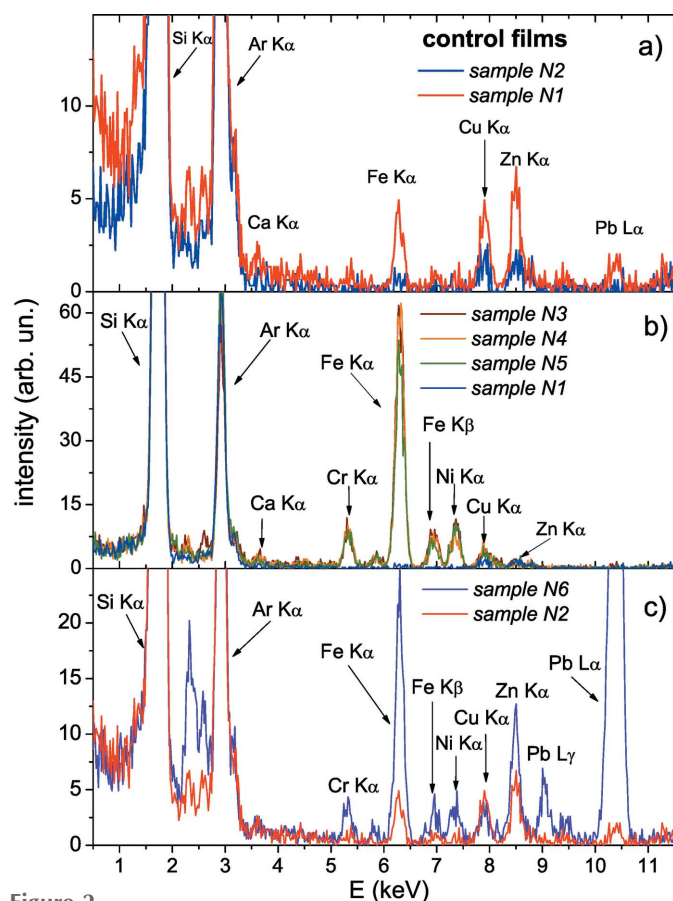


**Figure 2** Characteristic fluorescence spectra from protein films of alkaline phosphatase: (a) control films; (b) films of alkaline phosphatase exposed to chelating drug compounds at high concentrations which are toxic compared with therapeutic doses; (c) films of alkaline phosphatase exposed to a lead acetate solution. All spectra presented in this figure are normalized to acquisition time and the intensity of the incident beam.

immobilization power of cellulose acetopivalinate that is evidently demonstrated in AFM studies (Fig. 3) that were additionally performed in order to examine the surface morphology of the control samples. As can be seen in Fig. 3(a), AP molecules are arranged as single linear associates on sample N1 when a lipid monolayer was used for protein immobilization. In contrast, AFM images of the protein films immobilized on cellulose acetopivalinate revealed that in these samples protein molecules are uniformly and densely packed over the surface. This is clearly visible on the AFM topographic image of ‘uncovered’ protein film without the topmost cellulose acetopivalinate layer (this sample was especially deposited for AFM measurements)

A very important observation to be made from the characteristic fluorescence spectra shown in Fig. 2 is the presence of a set of peaks from impurity metals Cu, Fe, Cr and Ni. Trace amounts of iron and copper ions have been detected already in control samples N1 and N2 (Fig. 2a). The intensity of the Fe  $K_{\alpha}$  peak on the spectra from the films exposed to chelating agents or a lead solution is much higher (Fig. 2b, Fig. 2c). Moreover, two additional peaks (Cr  $K_{\alpha}$  and Ni  $K_{\alpha}$ ) arise on these spectra. Quite remarkable is the identity of element

composition of impurities in samples N3–N7. Furthermore, as can be seen in Fig. 2(b), the spectra from the samples N3–N5 (AP was exposed to chelating agents) coincide entirely in shape.

It should be emphasized that the purity of triply distilled water, used in our experiments, has been tested by inductively coupled plasma mass and atomic emission spectrometry methods at the Analytical Test Center of the Institute of Mineral Raw Materials (Moscow, Russia). It was determined that the concentration of metal ions in triply distilled water was less than the detection limit ( $10^{-7}$ – $10^{-8}$  M). These studies allowed the presence of impurities in triply distilled water to be excluded. Thus the experimental results presented in Fig. 2 provide definite evidence that the ability of protein to bind metal ions increased substantially under xenobiotic exposure.

In order to explain these experimental results one should take into account that AP is a dimer molecule with a complex quaternary structure (see Fig. 1b). AP is a metalloprotein where metal ions are necessary for catalytic activity and for the stabilization of the native conformation. The active site of the monomer contains three metal ions: two zincs and one magnesium. Two asymmetric wedge-shaped monomers of AP

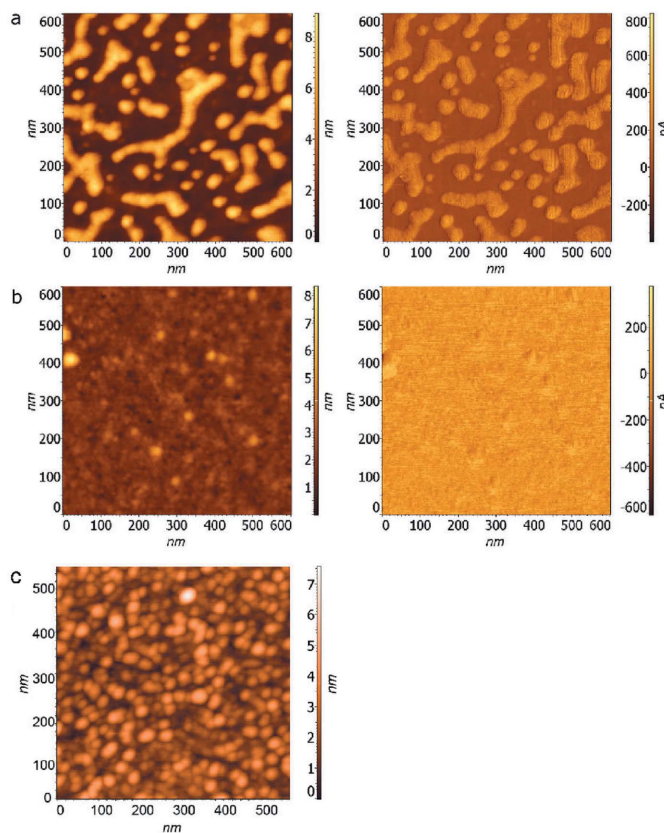


**Figure 3** Topographic and phase contrast images of the protein films. (a) Sample N1 (SI-L)+AP alkaline phosphatase was immobilized on the monolayer of the lipid mixture (phosphatidylcholine/cholesterol). (b) Sample N2 (SI-CAP)+AP alkaline phosphatase was immobilized on the monolayer of cellulose acetopivalinate. (c) ‘Uncovered’ protein film: the film was deposited in much the same way as sample N2 but without the topmost cellulose acetopivalinate layer.

interact with each other through a so-called conformational 'lock' composed of three spatially separated inter-subunit contact sites: I–III, II–II and III–I (Poltorak *et al.*, 1999; Chukhrai & Atyaksheva, 2010). Two identical contact sites I–III and III–I are located at the periphery. The most durable contact site II–II is linked to the active sites of AP. Poltorak *et al.* (1999) proposed the inactivation mechanism of AP that suggests step-by-step disruption of the conformational 'lock' before the loss of enzyme activity. This process starts with the alteration of the peripheral contact sites and the formation of AP intermediates that remain active. On the next step the destruction of the contact site II–II causes reversible changes in the active site structure, resulting in the formation of a labile dimer that dissociates gradually into inactive monomers.

In order to elucidate the mechanism and kinetics of the AP inactivation by metals (Cu, Pb) and chelating agents (xydiphone, mediphone, EDTA, succimer), systematic studies were carried out by Atyaksheva *et al.* (2011). The inhibition of AP by copper and lead ions was found to proceed in a two-stage manner. The first stage corresponds to the non-competitive mechanism of copper or lead binding in the active sites of AP; in the second stage AP molecules bind copper or lead ions both in the active site and on the surface, *i.e.* the mixed mechanism of inhibition. Kinetic analysis of AP inhibition by the chelating agents showed that these compounds bind with zinc ions in the active sites of the enzyme.

In view of these results it is reasonable to suggest the following mechanism by which xenobiotics can increase the ability of protein to bind metals. Incorporation of xenobiotic molecules (chelating agents or lead) into the active site of AP induces structural rearrangements of the ligand environment in this region. According to the inactivation mechanism of AP described by Poltorak *et al.* (1999), these rearrangements might cause the destabilization of the conformational 'lock' and open a rather large interface domain between two protein subunits. These changes will allow easy access to amino acid residues (usually buried), which have high metal-binding constants and can form complexes with metals even at the minute concentration of metal ions in the liquid subphase. It is clear that protein molecules perturbed by xenobiotics will bind a particular set of metal ions that are determined by the content of metal-coordinating residues and their spatial placement in the protein molecule. This explains the identity of element composition of impurity metals observed in two series of the protein films exposed to different reagents, *i.e.* chelating agents and a lead solution (samples N3–N5 and N6, N7). We would

like to particularly mention that the xenobiotic-induced changes discussed here are partial rearrangement of the AP native structure, but not a denaturation. This is shown by the experimental data obtained by Atyaksheva *et al.* (2011) where no loss of AP enzymatic activity was observed in the concentration range of chelating agents examined in the present studies.

### 3.2. Arrangement of metal ions in protein films

Important information on mechanisms of protein–metal binding can be extracted from the analysis of the angular dependence of the fluorescence yield shown in Figs. 4–6.

**3.2.1. Angular dependence of fluorescence yield from zinc ions.** The integrated intensity under the Zn  $K_{\alpha}$  peak is plotted as a function of the incident angle in Fig. 4. As discussed above, sufficiently intense Zn-fluorescence has been observed only on the samples N2 (SI-CAP)+AP and N6 {(SI-CAP)+AP}[Pb] where cellulose acetopivalinate was used as the immobilizing layer. The treatment of the experimental fluorescence curves has been performed using the well known recursive method developed by Parratt (1954). In the framework of this approach a stratified medium is described as a stack of homogeneous layers. For the analysis of the XSW fluorescence data obtained on samples N2 and N6, a three-layer model has been chosen: the bottom and the topmost layers, *i.e.* cellulose acetopivalinate monolayer, and the central layer, protein molecules. The thickness of the cellulose acetopivalinate monolayer was taken to be equal to the nominal

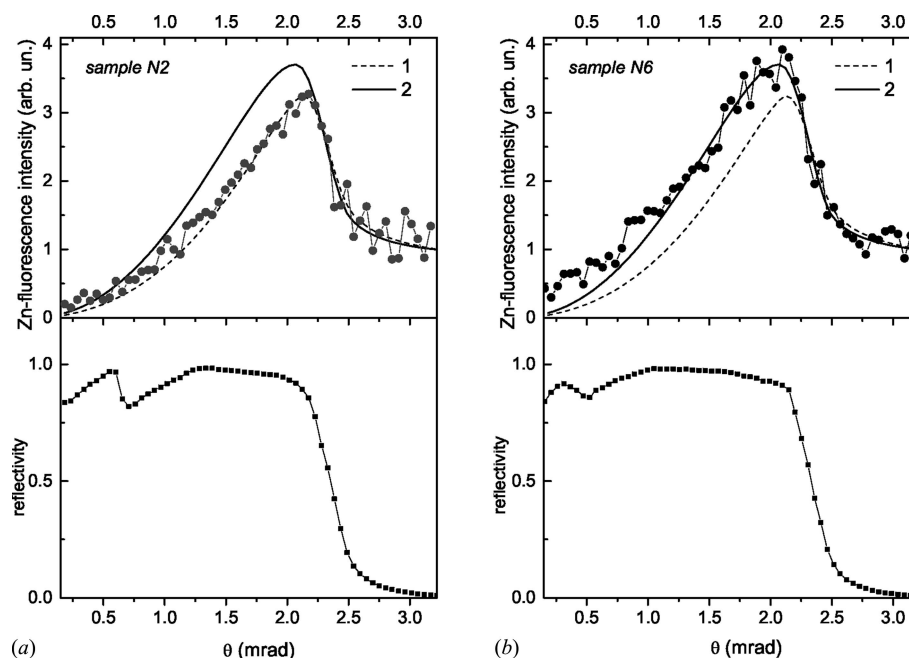


**Figure 4**

Angular dependence of reflectivity and Zn  $K_{\alpha}$  fluorescence yield from the protein films of alkaline phosphatase immobilized on the monolayer of cellulose acetopivalinate; samples N2 (SI-CAP)+AP (a) and sample N6 (SI-CAP)+AP[Pb] (b). Curve 1: the calculated angular dependence of the fluorescence yield from the film, in which zinc ions are distributed in a layer with a thickness of 10 Å at the bottom of the protein monolayer; curve 2: the calculated angular dependence of the fluorescence yield from the film, in which zinc ions are distributed over the whole thickness of the protein layer (50 Å).

size of the diameter of the polymer molecule, 13 Å. The Zn-fluorescence curves were fitted by varying the thickness and the position of the Zn layer.

Despite the general similarity of the Zn-fluorescence angular dependence in Fig. 4, noticeable distinction between these two curves is well defined: the maximum of the Zn-fluorescence curve obtained from sample N6 is broader and its position is shifted to smaller angles. This is a direct sign of the different width of the Zn ions distribution within the films. By fitting the experimental XSW data we estimated that in control sample N2 zinc ions are present in a thin layer with a thickness of  $10 \pm 2$  Å at the bottom of the protein monolayer. This information on zinc distribution is quite remarkable indicating that protein molecules form a well ordered layer, where AP molecules are oriented in such a way that active sites are facing the first polymer monolayer deposited on the solid substrate. Note that in this case the long axis of the ellipsoid of the protein molecule is directed along the solid substrate, as illustrated in Fig. 1(a).

Taking into account the protein dimensions of  $90 \times 50 \times 50$  Å, we expect the thickness of the protein layer to be  $\sim 50$  Å.

In sample N6 (the protein film was exposed to a lead acetate solution at a concentration of  $3 \times 10^{-4}$  M), the zinc distribution is much broader,  $\sim 50 \pm 10$  Å. This value is consistent with the thickness of the AP monolayer, and therefore one can conclude that, in sample N6, zinc ions are bound over the whole protein molecule. A possible explanation of the XSW data observed in this sample is that additional Zn-binding sites (outside the active site) appear on the AP molecule exposed to the lead solution.

**3.2.2. Angular dependence of fluorescence yield from lead ions.** A comparison of Pb  $L_{\alpha}$  fluorescence angular dependencies from protein films exposed to a lead solution (samples N6 and N7) reveals fundamental differences in the lead ions arrangement in these films. At a low concentration of  $3 \times 10^{-6}$  M (sample N7 {(SI-L)+AP}[Pb]), the angular dependence of the fluorescence yield from lead is sharply peaked in the vicinity of the critical angle for the substrate (Fig. 5a). This curve has been fitted using a two-layer model: the bottom layer being the lipid monolayer, and the upper layer the protein molecules. From the best fit the width of the lead ions distribution was found to be  $50 \pm 12$  Å and the thickness of the lipid layer was estimated to be  $15 \pm 5$  Å. The experimental curve of the Pb  $L_{\alpha}$  fluorescence from sample N6 {(SI-CAP)+AP}[Pb], when the concentration of lead ions in the solution was much higher ( $3 \times 10^{-4}$  M), exhibits absolutely different behavior; this angular dependence repeats the X-ray

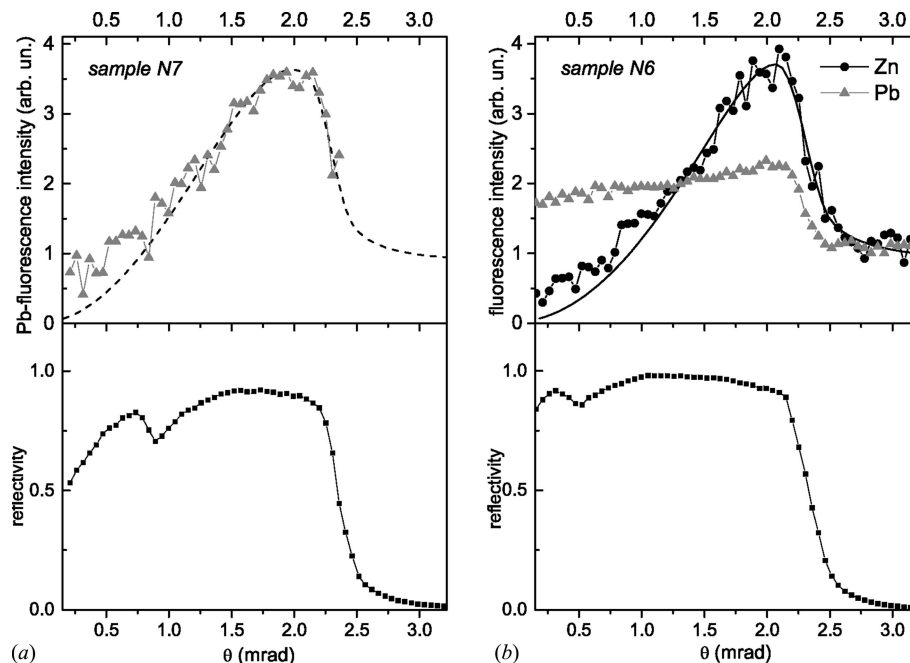


**Figure 5** Angular dependence of reflectivity and Pb  $L_{\alpha}$  fluorescence yield from the protein films of alkaline phosphatase exposed to a lead solution. (a) Sample N7 (SI-L)+AP[Pb]. The dashed curve represents the calculated angular dependence of the fluorescence yield from the film, in which lead ions are distributed over the whole thickness of the protein monolayer (50 Å). (b) Sample N6 (SI-CAP)+AP[Pb]. For comparison, the angular dependence of the Zn  $K_{\alpha}$  fluorescence yield from sample N6 is also shown.

reflectivity curve and takes the shape  $1 + R$  ( $R$  is the reflectivity squared amplitude). This kind of fluorescence curve can be attributed to the specific features of the lateral arrangement of the lead ions: they are arranged as discrete associates (Novikova *et al.*, 2009). These results give a clear hint as to the binding mechanisms of lead onto AP molecules: first, lead ions bond on the surface of the protein molecule and penetrate into the active sites of the enzyme. At higher concentration lead ions join in associates while the lead ions bound to the protein at the early stage serve as nuclei of association.

**3.2.3. Angular dependence of fluorescence yield from impurity ions.** The fluorescence curves from the impurity ions (Fe, Ni and Cr) have the shape  $1 + R$  [only the most intensive Fe fluorescence curve is shown in Fig. 6(b)]. As discussed above, these results suggest that impurity metal ions did not form a homogeneous layer but rather isolated grains. The experimental data for copper stand somewhat apart: copper ions were detected in all samples even in the control films. Remarkably, the intensity of the Cu  $K_{\alpha}$  peak did not increase in films exposed to a lead solution or chelating agents (see Figs. 2b, 2c). The intensity of the Cu  $K_{\alpha}$  peak in all films was too low and we failed to obtain estimations for the thickness of copper ions distribution. Nevertheless, even a qualitative consideration of the Cu fluorescence curves provides important information on the copper ions arrangement in the protein films. The angular dependence of the fluorescence yield from copper in all samples monotonically increases starting from zero at  $\theta = 0$  mrad and reaches a maximum value at the critical angle of TER for the substrate,

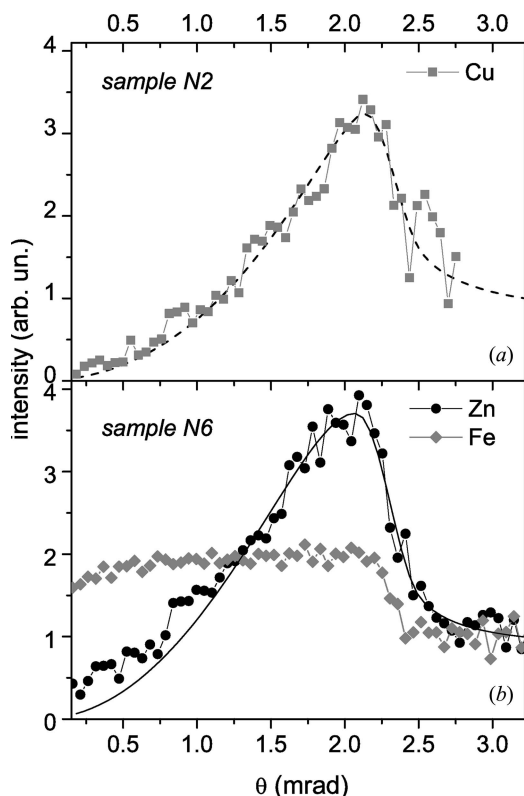


Figure 6

Angular dependence of the fluorescence yield from trace impurity metals (Cu and Fe) in the protein films of alkaline phosphatase. (a) Cu  $K_{\alpha}$  fluorescence yield from sample N2 (SI-CAP)+AP. The dashed curve represents the calculated angular dependence of the fluorescence yield from the film, in which copper ions are distributed in a layer with a thickness of 10 Å at the bottom of the protein monolayer. (b) Fe  $K_{\alpha}$  fluorescence yield from sample N6 (SI-CAP)+AP[Pb]. For comparison, the angular dependence of the Zn  $K_{\alpha}$  fluorescence yield from sample N6 is also shown.

that is a classic shape observed for thin films in the TER region. This suggests that a lateral distribution of copper ions can be considered as a continuous layer, in contrast to iron, nickel and chromium. These essential differences in lateral distribution of impurity metal ions point clearly to the fact that the mechanism of the protein–metal interaction depends on the type of metal ions.

#### 4. Conclusions

The XSW technique has been applied to study ordered protein films of AP exposed to different xenobiotic solutions: lead acetate solution and three drug compounds at high (compared with therapeutic doses) concentrations. The X-ray fluorescence measurements revealed considerable enhancement of the metal binding ability of AP induced by xenobiotics. It was established that after exposure to xenobiotic solutions protein films accumulated a set of metal ions (Fe, Cu, Cr, Ni) from triply distilled water in which metal contamination concen-

tration did not exceed  $10^{-7}$ – $10^{-8}$  M. Analysis of the angular dependence of the corresponding fluorescence yield provided information on the arrangement of trace metal ions in protein films. The presented experimental data can be explained by the partial rearrangement of native AP structure, namely destruction of a so-called conformational ‘lock’. In turn, such structural changes might result in uncovering a large interface domain between two AP subunits and make easily accessible amino acid residues which possess a rather high metal-binding strength.

The results obtained in these studies as well as in our earlier experiments give new insights into the molecular mechanisms of the disturbance of microelement balance in living organisms observed in metabolic diseases accompanied by endogenous or exogenous intoxication. In such cases the products of metabolic disorders might act as toxic agents that destabilize the native conformation of protein molecules and increase considerably the ability of protein molecules to bind metals.

#### Acknowledgements

This work was supported by the Russian Foundation of Fundamental Research, grant N14-22-01078.

#### References

- Atyaksheva, L. F., Chukhrai, E. S., Stepina, N. D., Novikova, N. N. & Yur'eva, E. A. (2011). *Russ. J. Phys. Chem.* **85**, 1084–1090.
- Batterman, B. (1964). *Phys. Rev.* **133**, 759–764.
- Bedzyk, M., Bilderback, D., Bommarito, G., Caffrey, M. & Schildkraut, J. (1988). *Science*, **241**, 1788–1791.
- Chukhrai, E. S. & Atyaksheva, L. F. (2010). *Russ. J. Phys. Chem.* **84**, 805–818.
- Iida, A., Matsushita, T. & Ishikawa, T. (1985). *Jpn. J. Appl. Phys.* **24**, L675–L678.
- Kovalchuk, M. V. & Kohn, V. G. (1986). *Sov. Phys. Usp.* **149**, 69–103.
- Libera, J. A., Cheng, H., Olvera de la Cruz, M. & Bedzyk, M. J. (2005). *J. Phys. Chem. B*, **109**, 23001–23007.
- Novikova, N. N., Kovalchuk, M. V., Stepina, N. D., Konovalov, O. V., Yurieva, E. A. & Chukhrai, E. S. (2011). *J. Surf. Invest.* **5**, 816–821.
- Novikova, N. N., Kovalchuk, M. V., Yur'eva, E. A., Konovalov, O. V., Rogachev, A. V., Stepina, N. D., Sukhorukov, V. S., Tsaregorodtsev, A. D., Chukhrai, E. S. & Yakunin, S. N. (2012). *Crystallogr. Rep.* **57**, 648–655.
- Novikova, N. N., Zheludeva, S. I., Stepina, N. D., Tolstikhina, A. L., Gaynutdinov, R. V., Haase, W., Erko, A. I., Knyazev, A. A. & Galyametdinov, Yu. G. (2009). *Appl. Phys. A*, **94**, 461–466.
- Parratt, L. G. (1954). *Phys. Rev.* **95**, 359–369.
- Poltorak, O. M., Chukhrai, E. S., Kozlenkov, A. A., Chaplin, M. F. & Trevan, M. D. (1999). *J. Mol. Catal. B*, **7**, 157–163.
- Templeton, A. S., Trainor, T. P., Traina, S. J., Spormann, A. M. & Brown, G. E. (2001). *Proc. Natl Acad. Sci. USA*, **98**, 11897–11902.
- Vartanyants, I. A. & Kovalchuk, M. V. (2001). *Rep. Prog. Phys.* **64**, 1009–1084.
- Wang, J., Wallace, C., Clark-Lewis, I. & Caffrey, M. (1994). *J. Mol. Biol.* **237**, 1–4.
- Zheludeva, S. I., Kovalchuk, M. V. & Novikova, N. N. (2001). *Spectrochim. Acta B*, **56**, 2019–2026.